ISSN 0036-0236, Russian Journal of Inorganic Chemistry, 2009, Vol. 54, No. 11, pp. 1689–1696. © Pleiades Publishing, Inc., 2009.
Original Russian Text © V.K. Ivanov, O.S. Polezhaeva, G.P. Kopitsa, P.P. Fedorov, K. Pranzas, V.V. Runov, 2009, published in Zhurnal Neorganicheskoi Khimii, 2009, Vol. 54, No. 11, pp. 1767–1775.

SYNTHESIS AND PROPERTIES OF INORGANIC COMPOUNDS

Specifics of High-Temperature Coarsening of Ceria Nanoparticles

V. K. Ivanov[a], O. S. Polezhaeva[a], G. P. Kopitsa[b], P. P. Fedorov[c], K. Pranzas[d], and V. V. Runov[b]

[a] *Kurnakov Institute of General and Inorganic Chemistry, Russian Academy of Sciences, Leninskii pr. 31, Moscow, 119991 Russia*

[b] *Konstantinov Institute of Nuclear Physics, Russian Academy of Sciences, Gatchina, Leningrad oblast, 188300 Russia*

[c] *Laser Materials and Technology Center, Prokhorov Institute of General Physics, Russian Academy of Sciences, ul. Vavilova 38, Moscow, 119991 Russia*

[d] *GKSS Research Centre, Geesthacht, Germany*

Received March 3, 2009

Abstract—Particle coarsening trends at high temperatures (200 to 700°C) in CeO_2 nanoparticles having various chemical histories are determined by powder X-ray diffraction (XRD), low-temperature nitrogen adsorption, transmission electron microscopy, and small-angle neutron scattering (SANS). Intergrowth of individual CeO_2 crystallites is the main scenario of nanoparticle coarsening.

DOI: 10.1134/S0036023609110023

Nanocrystalline ceria is a unique multipurpose material widely used in industries. In particular, ceria is used in protective coatings for absorption and redistribution of UV radiation, as the main component of polishing compositions and abrasives, including those used for chemomechanical surface treatment of silicon wafers in micro- and nanoelectronics, in catalytic systems, in trace gas sensors, in protective coatings for metals and alloys, and in other fields [1–5].

Ceria-based materials, including oxygen sensors and car emission converters, in some cases perform at temperatures above 600°C because of substantially higher oxygen mobilities in crystal lattices at these temperatures. Cerium ions have relatively moderate diffusive mobilities at these temperatures; in particular, the volume diffusion of cerium ions is not observed when thin-film CeO_2 samples are heated to 627°C [6], unlike, for example, titanium(IV) ion diffusion in titania thin films. Nonetheless, in spite of low cation mobilities, the high-temperature performance of CeO_2 nanomaterials is inevitably accompanied by noticeable particle coarsening and reduction in the specific surface area of the material (see, e.g., [7, 8]). Presumably, ceria particle coarsening under heating is due to cooperative mass transfer processes involving mutual movement and rotation of CeO_2 crystallites as a whole more than due to thermally activated diffusion processes. In particular, a similar compaction scenario was earlier observed in the shrinkage of so-called reactive metal powders with linear particle sizes on the order of 100 nm at moderate temperatures [9]. However, direct experimental evidence for particle coarsening mechanisms in CeO_2 nanopowders has been lacking until now.

This work studies particle-size variation trends in ceria nanopowders having various chemical histories upon heating within 200–700°C and determines the prevalent scenario of CeO_2 particle coarsening.

EXPERIMENTAL

Rapid and homogeneous hydrolysis processes described below were used to prepare ceria nanopowder samples.

Rapid hydrolysis involved precipitating CeO_2 by addition of aqueous ammonia to aqueous–isopropanolic solutions of $Ce(NO_3)_3$ [10, 11]. Cerium(III) nitrate (0.08 mol/L) solutions in aqueous isopropanol with water/isopropanol (vol/vol) ratios of 1 : 1, 1 : 3, and 1 : 19 were rapidly added with vigorous stirring to aqueous ammonia (3 mol/L) taken in a fivefold molar excess and kept for 2 h at room temperature. Precipitates were washed with isopropanol three times and dried at 60°C for 2 h.

Homogeneous hydrolysis in the presence of urea involved the reaction of ammonium hexanitratocerrate(IV) $(NH_4)_2[Ce(NO_3)_6]$ with ammonium hydroxide generated by hydrolysis of aqueous urea solutions. Aqueous solutions of $(NH_4)_2[Ce(NO_3)_6]$ and urea were mixed in the ratio 1 : 2 (mol/mol) (the ammonium hexanitratocerrate(IV) concentration was 0.05, 0.15, and 0.4 mol/L) and brought to boiling in a Linn High Therm laboratory microwave furnace at the 800 W power; then, the heating power was reduced to 300 W, and the

Synthesis parameters and notations of ceria samples

Sample notation	Synthesis parameters	Annealing temperature, °C	Annealing time, h
Ce-1-1	Rapid precipitation by aqueous ammonia from an aqueous–isopropanolic (1 : 1) solution of $Ce(NO_3)_3 \cdot 6H_2O$	200, 300, 400, 500, 600, 700	2, 4, 6, 8
Ce-1-2	Rapid precipitation by aqueous ammonia from an aqueous–isopropanolic (1 : 3) solution of $Ce(NO_3)_3 \cdot 6H_2O$	200, 300, 400, 500, 600, 700	2
Ce-1-3	Rapid precipitation by aqueous ammonia from an aqueous–isopropanolic (1 : 19) solution of $Ce(NO_3)_3 \cdot 6H_2O$	200, 300, 400, 500, 600, 700	2
Ce-1-4	Rapid precipitation by aqueous ammonia from an aqueous solution of $Ce(NO_3)_3 \cdot 6H_2O$	200, 300, 400, 500, 600, 700	2
Ce-1-5	Rapid precipitation by aqueous ammonia from an aqueous solution o $Ce(NO_3)_3 \cdot 6H_2O$ followed by freeze drying	200, 300, 400, 500, 600, 700	2
Ce-2-1	Homogeneous microwave hydrolysis of $(NH_4)_2[Ce(NO_3)_6]$ (0.05 mol/L) in the presence of urea	400, 500	2
Ce-2-2	Homogeneous microwave hydrolysis of $(NH_4)_2[Ce(NO_3)_6]$ (0.15 mol/L) in the presence of urea	300, 400, 500, 700	2, 4, 6, 8
Ce-2-3	Homogeneous microwave hydrolysis of $(NH_4)_2[Ce(NO_3)_6]$ (0.4 mol/L) in the presence of urea	300, 400, 500, 700	2

boiling mixture was kept for 0.5 h. The volume of the treated solution was 450 mL in all experiments. The resulting precipitates were washed with water three times, centrifuged, and dried at 60°C for 2 h.

For the recognition of trends of ceria nanoparticle coarsening during heat treatment, the samples prepared by rapid and homogeneous hydrolysis were annealed in air at 200, 300, 400, 500, 600, and 700°C for 2 h at each temperature (table). Some samples were additionally annealed at the same temperatures for 4, 6, and 8 h. The samples were brought to the isothermal exposure temperature at a rate of 5 K/min.

In addition, experiments were carried out to prepare ceria with the use of freeze drying. A ceria pulp precipitated by aqueous ammonia from an aqueous cerium(III) nitrate solution was washed with distilled water three times and divided into two parts. One part was freeze dried. The other (serving as a blank) was dried at 60°C for 2 h. Freeze drying was carried out in a Labconco FreeZone freeze drier with gradual temperature elevation from –30 to +30°C at 1 kPa pressure. Both sets of samples were then annealed at 200, 300, 400, 500, 600, and 700°C for 2 h.

Powder X-ray diffraction analysis was carried out on a Rigaku D/MAX 2500 diffractometer (CuK_α radiation); the goniometer rotation speed was 1 deg/min. Diffraction peaks were identified with reference to the JCPDS database. Fine crystal structure parameters for ceria were determined by X-ray diffraction. Coherent scattering lengths d_{CSL}s were determined from the Selyakov–Scherrer relationship

$$d_{CSL} = \frac{\lambda}{\beta \cos\theta}, \quad (1)$$

where $\lambda_{Cu} = 1.54178$ Å and β is physical broadening of the (111) diffraction peak from ceria. A sapphire single crystal was used as a reference to apply correction for instrumental broadening.

Microstructure was observed using transmission electron microscopy (TEM) on a Leo912 AB Omega electron microscope at an accelerating voltage of 100 kV. Test samples were placed on polymer-film-coated 3.05-mm copper grids.

Specific surface areas of CeO_2 powders were measured by low-temperature nitrogen adsorption using a QuantaChrome Nova 4200B analyzer. Before measurements, test samples were degassed for 5 h in a drying compartment at 40°C under vacuum. Surface analysis was carried out using the multipoint (28 points) Brunauer–Emmet–Teller (BET) method. Pore-size dis-

tributions were calculated from nitrogen desorption isotherms using the Barrett–Joyner–Halenda (BJH) method. The Neimark–Kiselev method [12, 13] was used in surface fractal analysis.

Thermogravimetric analysis (TGA) and differential thermal analysis (DTA) were carried out on a Perkin Elmer TG7 thermal analyzer in a polythermal mode (heating in air at 5 K/min to 1150°C).

Small-angle neutron scattering (SANS) was measured on a SANS-2 setup (FRG1 reactor, GKSS Research Centre, Geesthacht, Germany) at the neutron wavelength $\lambda = 5.8$ Å, $\Delta\lambda/\lambda = 10\%$. The experiments were carried out at four sample–detector distances (SD = 1, 3, 9, and 20.7 m), which allowed neutron scattering intensities to be measured in the range of moment transfers $1.7 \times 10^{-3} < q < 2.5 \times 10^{-1}$ Å^{-1}. Scattered neutrons were detected by a ^{3}He position-sensitive area detector.

CeO_2 nanopowder samples were placed to quartz cells 1 mm thick. Initial spectra for each q range were corrected using a standard procedure [14] for the scattering from the setup hardware, cell, and ambience. The thus-obtained two-dimensional isotropic spectra were azimuthally averaged and reduced to absolute magnitudes via scaling to the vanadium incoherent scattering cross section with account for the detector efficiency [14] and bulk density ρ_H for each sample. All measurements were carried out at room temperature.

The SANS intensity $I_s(q)$ was determined as

$$I_s(q) = I(q) - TI_0(q), \quad (2)$$

Here, $I(q)$ and $I_0(q)$ are the q distributions of scattering neutrons after transmission through the sample and the beam without test samples, respectively; and T is the transmission coefficient for neutrons transmitted through the sample:

$$T = I/I_0 = e^{(-\Sigma L)}, \quad (3)$$

where $\Sigma = \sigma_s + \sigma_a$ is the integral cross section, including the nuclear scattering σ_s and absorption σ_a, and L is the sample thickness.

The SANSFIT program [15] was used to transform SANS curves to particle-size distribution functions.

RESULTS AND DISCUSSION

Analysis of As-Synthesized (Unannealed) CeO_2 Samples

All samples prepared by rapid or homogeneous hydrolysis were identified as single-phase ceria with fluorite structure using powder X-ray diffraction. The coherent scattering lengths in CeO_{2-x} calculated from (111) diffraction peak broadening were 3.5 nm for the samples prepared by homogeneous hydrolysis in the presence of urea and 4.5 nm for the samples prepared by rapid hydrolysis. Thus, the preparation process only insignificantly affects CeO_2 particle sizes.

Transmission electron microscopy shows that the samples prepared by rapid or homogeneous hydrolysis are heavily aggregated powders with particle sizes of 4–5 nm (rapid precipitation) and 2–3 nm (homogeneous hydrolysis in the presence of urea).

TGA weight loss curves recorded upon heating for CeO_2 samples prepared from aqueous isopropanol are virtually the same regardless of isopropanol concentrations; the overall weight loss reaches 15%. Adsorbate water is eliminated in the range 25–100°C with an endotherm. Heating to higher temperatures does not give rise to any considerable heat effect.

For the ceria samples prepared by rapid hydrolysis in the presence of urea, the weight loss curves upon heating are also virtually the same; most weight loss (reaching 15%) is observed within 250–300°C; DTA curves show a well-defined exotherm, whose appearance can be assigned to the decomposition of residual cerium compounds, including cerium(III) hydroxocarbonate, and simultaneous CeO_2 crystallization.

Low-temperature nitrogen adsorption shows that, as the isopropanol percentage in the starting solutions increases from 50 to 95%, the specific surface area of CeO_2 nanopowders decreases from 220 to 110 m^2/g. For the samples prepared by homogeneous hydrolysis in the presence of urea, specific surface areas are almost unaffected by the starting solution composition and range from 85 to 96 m^2/g.

Analyses of CeO_2 Samples after High-Temperature Annealing

Annealing of the samples prepared by rapid hydrolysis at 200–700°C for 2 h gives rise to a systematic increase in CSL size from 3–4 to 22–24 nm as shown by powder X-ray diffraction. The CeO_2 powders prepared by hydrolysis in the presence of urea behave in a similar way; in this case, however, the final CSL sizes are 19–20 nm (Fig. 1).

Examination of the CSL size versus annealing time curves measured at fixed temperatures for ceria samples having different chemical histories (Fig. 2) indicates that the particle size is time-independent to the measurement error over the range of the temperatures studied (up to 700°C).

The observed constancy of CSL sizes at fixed temperatures appreciably differs from the classical diffusive ripening model, which obeys the parabolic law

$$D^2 - D_0^2 = k\tau, \quad (4)$$

and is driven by the excessive surface energy, the latter being a function of particle curvature radii. Similar results gave the study of grain-growth dynamics in CeO_2 and $Ce_{0.78}Gd_{0.22}O_{1.89}$ thin films prepared by aerosol pyrolysis [16]. Presumably, the constancy of particle sizes regardless of increasing treatment time and their coarsening in response to increasing annealing

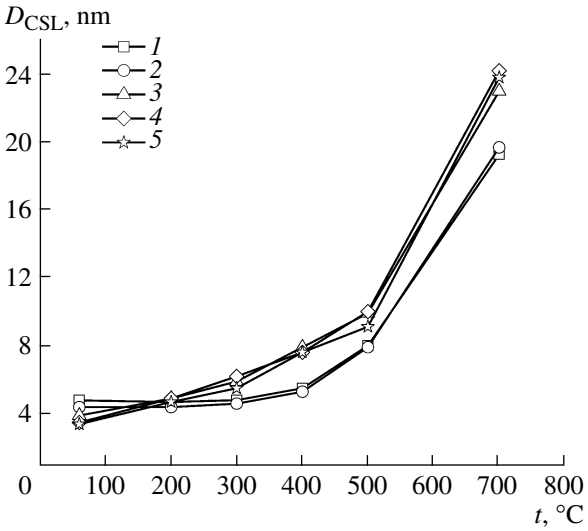

Fig. 1. Ceria particle size in samples with various chemical histories vs. annealing temperature. Samples: (*1*) Ce-1-1, (*2*) Ce-1-3, (*3*) Ce-2-1, (*4*) Ce-2-2, and (*5*) Ce-2-3.

temperature are due to the operation of the threshold crystallite intergrowth mechanism, like the one described for the sintering of coarse-grained materials [9]. CeO_2 crystallites newly formed during the synthesis are aggregated to form a whole spectrum of high-angle and low-angle boundaries. Various types of stoppers (surface defects, contacts with other particles, and so on) inhibit a free movement of crystallites relative to one another; as temperature elevates, stopper thresholds are crossed, the proportion of mutually aligned particles at each temperature being determined by both the starting state of the powder and the heat energy supply. Roughly, the scenario is as follows: at relatively low temperatures, the rotation of particles with the least misalignment occurs; at higher temperatures, mutual movement of more strongly misaligned crystallites occurs, and so on. Subsequent merging of aligned particles to a larger particle occurs via surface (grain-boundary) diffusion.

For ascertaining apparent diffusion coefficients, we carried out additional short-term anneals of sample Ce-1-1 at 700°C for 5, 10, 20, and 60 min.

The results of these anneals show that particle coarsening at the chosen annealing temperature has the highest rate during the first ten minutes and then CSL sizes change only insignificantly. The description of the coarsening dynamics using the relaxation function employed in [16, 17] for analysis of the self-confined coarsening of nanoparticles, allowed the relaxation time to be determined as $\tau_1 \approx 7$ min. This is roughly 30 times smaller than the respective value determined for $Ce_{0.78}Gd_{0.22}O_2$ nanocrystalline films during 700°C isothermal annealing [16]. In turn, a value of 2.2×10^{-19} m^2/s was calculated for the apparent diffusion coefficient from this relaxation time, as in [16, 17], exceeding the

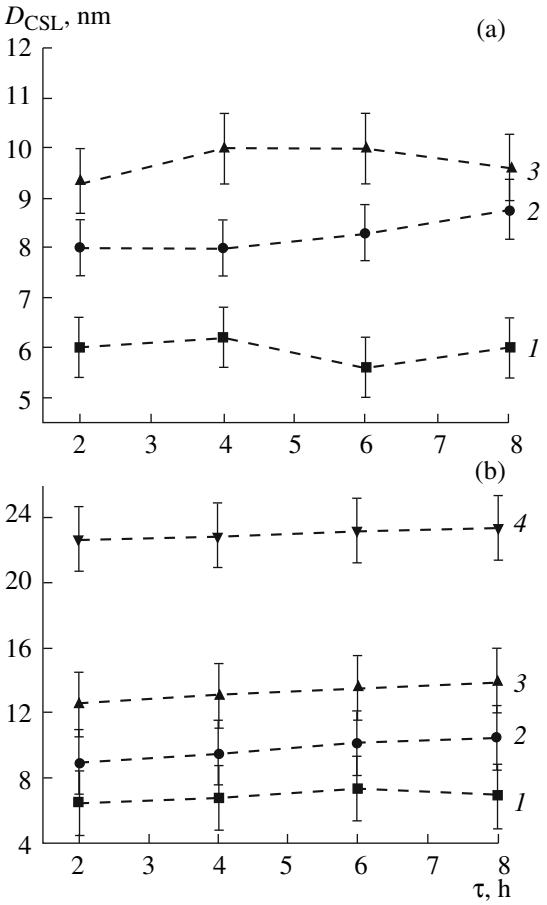

Fig. 2. CSL size vs. annealing time for (a) sample Ce-2-3 annealed at (*1*) 300, (*2*) 400, and (*3*) 500°C and (b) sample Ce-1-1 annealed at (*1*) 400, (*2*) 500, (*3*) 600, and (*4*) 700°C.

value found in [16] by more than two orders of magnitude. Taking as the basic hypothesis that crystallite coarsening occurs via mutual attachment and subsequent intergrowth, we may infer that strong contacts between particles and the substrate in films hinder particle realignment and slows down nanoparticle growth rates compared to CeO_2 nanopowders.

Recall that different versions of nanocrystalline ceria synthesis yield samples with different specific surface area values. Presumably, such samples will behave differently during high-temperature annealing. To check this presumption, we carried out isothermal anneals of samples prepared by rapid precipitation from aqueous–isopropanolic solutions of cerium(III) nitrate with various isopropanol proportions (1 : 1 and 1 : 3). Figure 3 displays the resulting S_{sp} versus annealing temperature curves.

The elevating annealing temperatures systematically decrease the specific surface areas of both samples; the $S_{sp}(T)$ trend is substantially dictated by the sample history. Inasmuch as particle sizes in the as-synthesized samples were practically the same, we can infer that, to a considerable extent, the aggregation and

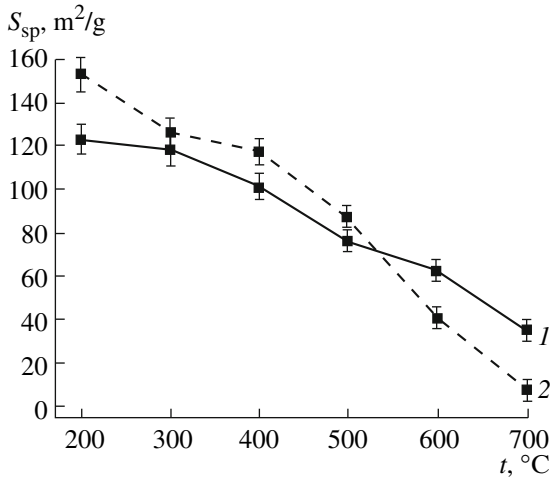

Fig. 3. Specific surface area vs. isothermal annealing temperature for samples with various chemical histories. Samples: (*1*) Ce-1-2 and (*2*) Ce-1-1.

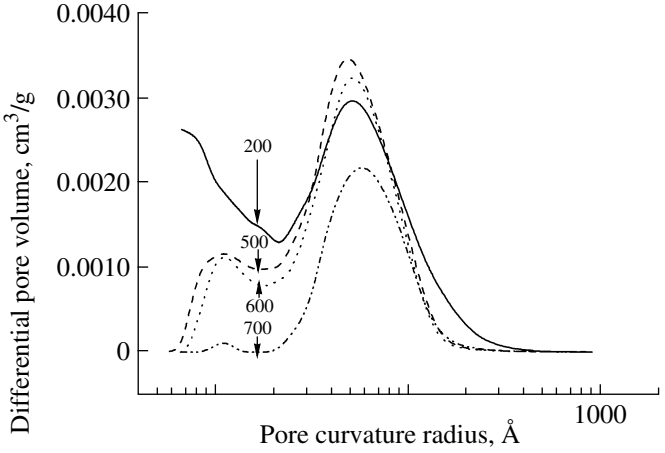

Fig. 4. Differential pore volume vs. annealing temperature for sample Ce-1-2. Temperatures in degrees Celsius are indicated at the plot.

mutual arrangement of particles determine the particle coarsening dynamics.

Low-temperature nitrogen adsorption indicates that sample Ce-1-1 contains a far greater percentage of small-size pores; this implies a greater contribution from low-angle grain boundaries to the overall porosity of the CeO_2 sample. The Neimark–Kiselev analysis of low-temperature nitrogen adsorption data indicates that this sample has a greater value of fractal surface dimension in the range from 0.2 to 3.5 nm (D = 2.66 and 2.57 nm for samples Ce-1-1 and Ce-1-2, respectively). This is another piece of evidence in favor of the greater contribution of small-size pores, which are generated by low-angle contacts of particles, to the overall porosity.

The differential pore volume versus annealing temperature curve plotted in Fig. 4 for sample Ce-1-2 implies that relatively small pores (with diameters less than 0.25 nm) are the first to disappear upon heat treatment, whereas the position and height of the second pore-size distribution peak are far less changed. Thus, high-temperature annealing primarily eliminates low-angle boundaries between CeO_2 particles, in good match with the above-described particle coarsening model.

TEM images of samples Ce-1-, Ce-1-2, and Ce-1-3 show that annealing at temperatures below 400°C does not considerably change nanoparticle sizes or their aggregation character. Average particle sizes increase systematically upon annealing at 500–700°C, and this increase well correlates with the particle size versus annealing temperature relationship derived from X-ray diffraction data. We should mention that X-ray diffraction gives slightly overestimated particle size values.

The as-synthesized samples and the samples annealed at low temperatures (below 400°C) typically have sufficiently narrow particle size distributions. In turn, the samples annealed at high temperatures (500–700°C) are distinguished by polydisperse distributions. Comparison of the micrographs of the as-synthesized and annealed samples shows that particles whose sizes coincide with or insignificantly exceed the particle sizes in as-synthesized CeO_2 samples are conserved inside aggregates even for the highest annealing temperatures (Fig. 5). This fact is at variance with the Ostwald ripening model, which states that particle size coarsening is driven by the different surface curvature radii of particles. However, such the behavior of the system matches the oriented attachment model of particle coarsening; indeed, in terms of this model, considerable misalignment can hinder particle intergrowth even at high temperatures.

More support to the influence of particle aggregation on the high-temperature annealing behavior of samples was provided by a comparative study of the particle coarsening dynamics in ceria samples precipitated by aqueous ammonia from aqueous cerium(III) nitrate solutions and afterwards either dried in air (set a) or dehydrated by freeze drying (set b). Figure 6 displays the relevant XRD data for set a and set b samples.

X-ray diffraction shows equal particle sizes for the as-synthesized samples of both sets and for the samples annealed at temperatures below 500°C. When the annealing temperature increases to 600°C and 700°C, the particle sizes in the samples of the cryochemical set become noticeably smaller than for the reference samples. Transmission electron microscopy verifies the different particle coarsening dynamics (Fig. 7).

In our opinion, different aggregate structures of as-synthesized powders are responsible for different particle coarsening dynamics. Indeed, when wet $CeO_2 \cdot xH_2O$ powders are dried in an ordinary manner in air, water elimination from interparticle pores causes particles to come more closely to one another and gen-

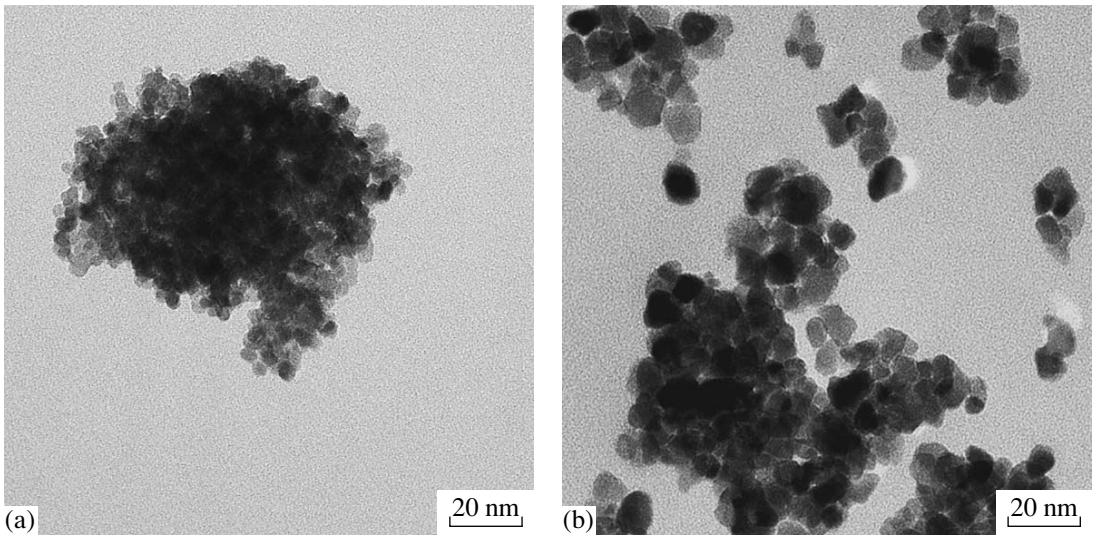

Fig. 5. Micrographs of samples prepared from aqueous–isopropanolic (1 : 1) solutions of cerium(III) nitrate and annealed at (a) 400°C and (b) 600°C.

erates low-angle boundaries. During freeze drying in the absence of a liquid phase, crystallites remain more disordered, which inhibits their subsequent intergrowth.

Small-angle neutron scattering was used to highlight more structural features of the as-synthesized ceria samples and the samples afterwards annealed at various temperatures. Figure 8 displays the log–log curves of scattering cross sections $d\Sigma(q)/d\Omega$ for the CeO_2 samples obtained by annealing sample Ce-1-1 at 60–700°C.

The examination of the SANS curves shown in Fig. 8 is useful for the restoration of the size distribution function for scattering inhomogeneities (particles):

$$D_V(R) = D_N(R)V, \quad (5)$$

Here, $D_N(R)$ is particle-radius distribution density function and V is particle volume.

Direct modeling of scattering curves using the form-factor of individual noninteracting spherical particles with account for the log-normal particle distribution function (which is usually used in practice) does not give reliable results, indicating a considerable polydispersion of particles in the system. Therefore, we used an indirect Fourier transformation [15, 18] for estimating the $D_V(R)$ function; this transformation is less sensitive to a break at small radii that occurs in real systems. Figure 9 displays the resulting particle-size distribution functions $D_V(R)$ for samples annealed at various temperatures. A good fit to experimental data is shown by the scattering curves restored from the $D_V(R)$ distributions (Fig. 8).

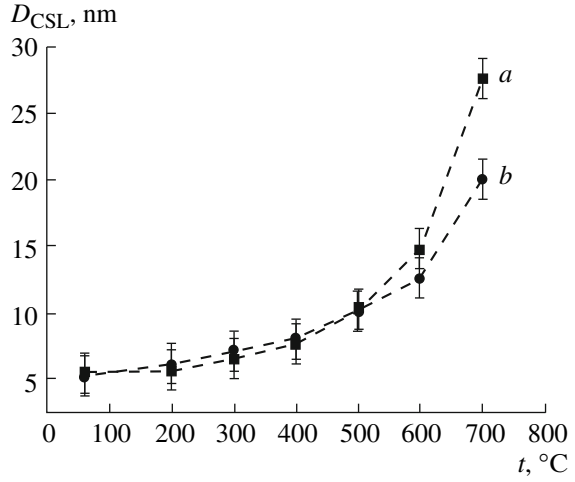

Fig. 6. CSL size vs. annealing temperature for (a) sample Ce-1-4 and (b) sample Ce-1-5.

The above data imply that an as-synthesized sample is characterized by a sufficiently narrow monomodal particle size distribution. Annealing at 200°C gives rise to a shoulder on the distribution curve, evidently, because of a partial dehydration of residual cerium hydroxo compounds and the associated systematic increase in CeO_2 particle size. The decomposition of the hydroxo compounds completely finishes at 400°C as probed by TGA; the particle size distribution again becomes monomodal, and the peak position on the distribution curve is displaced by~0.6 nm toward higher values from its position in the as-synthesized sample. Subsequent heat treatment at high temperatures (600–700°C), where particle coarsening is reliably detected by both XRD and TEM, gives rise to a bimodal particle-size distribution. The first peak on the distribution curve virtually retains its position, but the proportion of the

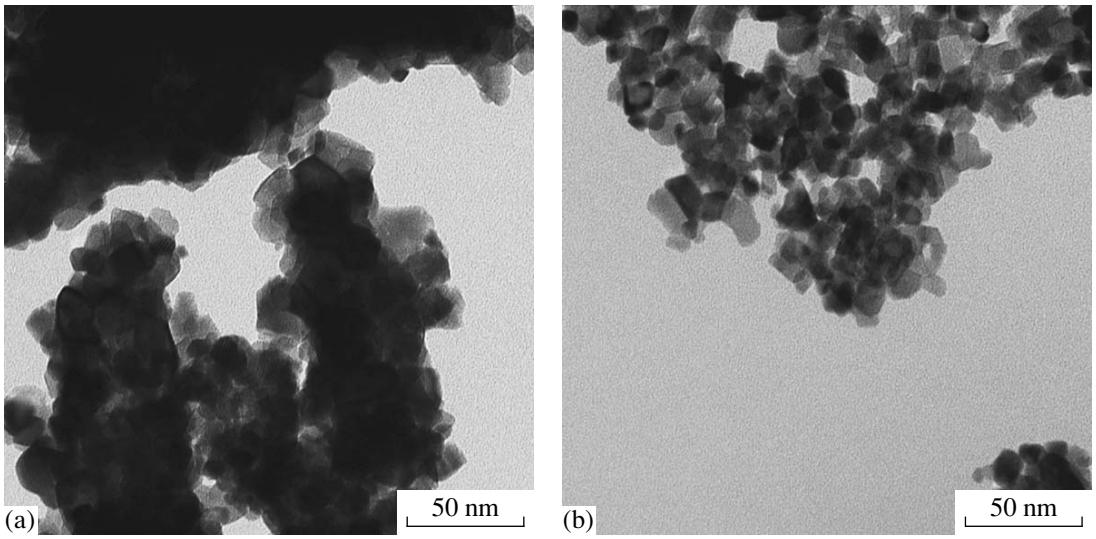

Fig. 7. Micrographs of ceria samples annealed at 700°C for 2 h. Samples: (a) Ce-1-4 and (b) Ce-1-5.

relevant particles decreases. The second peak shifts toward larger sizes and becomes more diffuse as temperature increases.

Small-angle neutron scattering shows that CeO_2 particles are grown via consecutive intergrowth rather than via Ostwald's ripening. Indeed, the occurrence of the first particle-size distribution peak in the samples annealed at 600 and 700°C means that small particles whose sizes correspond to the particle sizes of the as-synthesized samples survive even after a high-temperature annealing of CeO_2, but their proportion decreases. We should note that, if Ostwald's ripening operated, the main (first) particle-size distribution peak would have shifted and become diffuse, which is not actually observed.

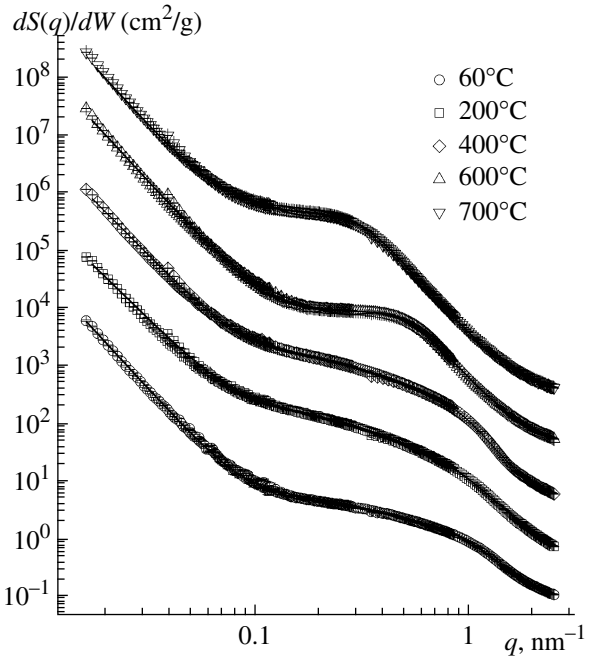

Fig. 8. SANS cross section $d\Sigma(q)/d\Omega$ for CeO_2 samples annealed at various temperatures vs. momentum transfer q. For better illustration, the curves are multiplied by 10 (for 200°C), 100 (400°C), 1000 (600°C), and 10 000 (700°C). Solid lines are the best-fit curves corresponding to the scattering particle size distribution $D_V(R)$ (see Fig. 9).

ACKNOWLEDGMENTS

This work was supported by the Russian Foundation for Basic Research (project no. 08-03-00471) and Program no. 27 of the Russian Academy of Sciences "Fun-

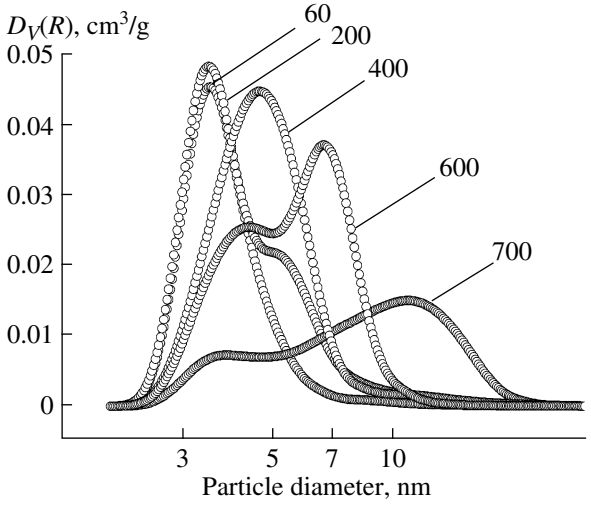

Fig. 9. Particle size distribution for sample Ce-1-1 annealed at various temperatures. Annealing temperatures in degrees Celsius are indicated at the plot.

damentals of Basic Research into Nanotechnologies and Nanomaterials."

REFERENCES

1. S. Yabe and T. Sato, J. Solid State Chem. **171**, 7 (2003).
2. N. Izu and W. Shin, Sensors and Actuators B: Chem. **113**, 207 (2006).
3. G. Panzera, V. Modafferi, S. Candamano, et al., J. Power Sources **135**, 177 (2004).
4. X. D. Feng, D. C. Sayle, Z. L. Wang, et al., Science **312**, 1504 (2006).
5. A. S. Hamdy, Mater. Lett. **60**, 2633 (2006).
6. C. L. Perkins, M. A. Henderson, C. H. F. Peden, and G. S. Herman, J. Vac. Sci. Technol., A **19**, 1942 (2001).
7. *Binary Rare Earth Oxides*, Ed. by G. Adachi, N. Imanaka, and Z. C. Kang (Kluwer, Dordrecht, 2004).
8. *Catalysis by Ceria and Related Materials* (Catal. Sci. Ser.), Ed. by A. Trovarelli (World Scientific Publishing Company, Singapore, 2002).
9. Ya. E. Geguzin, *Physics of Sintering* (Nauka, Moscow, 1984) [in Russian].
10. V. K. Ivanov, F. Yu. Sharikov, O. S. Polezhaeva, and Yu. D. Tret'yakov, Doklady Chem. **411**, 223 (2006).
11. V. K. Ivanov, O. S. Polezhaeva, G. P. Kopitsa, et al., Inorg. Mater. **44**, 272 (2008).
12. A. V. Neimark, Ads. Sci. Tech. **7**, 210 (1990).
13. A. V. Neimark, Pis'ma Zh. Eksp. Teor. Fiz. **51**, 535 (1990).
14. G. D. Wignall and F. S. Bates, J. Appl. Crystallogr. **20**, 28 (1986).
15. P. Biemann, M. Haese-Seiller, and P. Staron, Physica B **276—278**, 156 (2000).
16. J. L. M. Rupp, A. Infortuna, and L. J. Gauckler, Acta Mater. **54**, 1721 (2006).
17. J. F. Loffler and W. L. Johnson, Appl. Phys. Lett. **76**, 3394 (2000).
18. D. I. Svergun and L. A. Feigin, *Small-Angle Scattering of X-ray and Neutrons* (Nauka, Moscow, 1986) [in Russian].